Articles   Faculty Publications

7-9-2014

Slow Plastic Creep of 2D Dusty Plasma Solids

Angela Douglass
Ouachita Baptist University, douglassa@obu.edu

Peter Hartmann
Research Institute for Solid State Physics and Optics of the Hungarian Academy of Sciences

Aniko Zs. Kovacs
Institute for Solid State Physics and Optics

Jorge C. Reyes
Center for Astrophysics, Space Physics and Engineering Research

Lorin S. Matthews
Center for Astrophysics, Space Physics and Engineering Research

See next page for additional authors

Follow this and additional works at: https://scholarlycommons.obu.edu/articles

Part of the Physics Commons

Authors

Angela Douglass, Peter Hartmann, Aniko Zs. Kovacs, Jorge C. Reyes, Lorin S. Matthews, and Truell W. Hyde

Slow Plastic Creep of 2D Dusty Plasma Solids

Peter Hartmann,[1,2] Anikó Zs. Kovács,[1] Angela M. Douglass,[3]
Jorge C. Reyes,[2] Lorin S. Matthews,[2] and Truell W. Hyde[2]

[1]*Institute for Solid State Physics and Optics, Wigner Research Centre,
Hungarian Academy of Sciences, P.O.Box. 49, H-1525 Budapest, Hungary*
[2]*Center for Astrophysics, Space Physics and Engineering Research (CASPER),
One Bear Place 97310, Baylor University, Waco, Texas 76798, USA*
[3]*Ouachita Baptist University, 410 Ouachita Street, Arkadelphia, Arkansas 71923, USA*

We report complex plasma experiments, assisted by numerical simulations, providing an alternative
qualitative link between the macroscopic response of polycrystalline solid matter to small shearing forces
and the possible underlying microscopic processes. In the stationary creep regime we have determined the
exponents of the shear rate dependence of the shear stress and defect density, being $\alpha = 1.15 \pm 0.1$ and
$\beta = 2.4 \pm 0.4$, respectively. We show that the formation and rapid glide motion of dislocation pairs in the
lattice are dominant processes.

The direct *in situ* observation of dynamical processes in
bulk condensed matter is not yet available with atomic
resolution in both space and time. Femtosecond pump-
probe techniques can resolve atomic motion; atomic force
microscopy can detect atoms on surfaces; diffraction
methods provide information about the bulk structure;
but as long no method can combine all the benefits of
these techniques, we are limited to rely on phenomeno-
logical models and numerical simulations. Alternative
experimental methods have already proven to be helpful
for the qualitative understanding of classical collective
phenomena. Charged colloids suspended in a liquid envi-
ronment, and dusty plasmas (solid micron sized particles
charged and levitated in gas discharge plasmas) are both
interacting many-particle systems that show very similar
properties to conventional atomic matter, but at time and
distance scales easily and directly accessible with simple
video microscopy techniques. Both methods provide
insight into the microscopic (particle level) details of
different phenomena. Colloid systems are characterized
by over-damped dynamics, due to the liquid environment,
which makes them well suited for structural and phase
transition studies [1], while the weak damping in low
pressure gas discharges makes dusty plasmas perfect for
studies of wave dynamics, instabilities, and other collective
excitations [2].

In material science and metallurgy, creep is the time
dependent plastic strain at constant stress and temperature;
therefore, it is a special type of plastic deformation of solid
matter. In general it is a slow process driven by the
thermally activated movement of dislocations (dislocation
creep), vacancies (vacancy creep), or diffusion (Nabarro-
Herring and Coble creep). The applied stresses are below
the rapid yield stress resulting in atomic movements that are

crystallographically organized. The applied temperatures
are usually above $(1/2)T_m$, where T_m is the melting
temperature. The time (t) evolution of the deformation
(strain ε) at constant stress is often described by one of the
empirical formulas

$$\varepsilon = \varepsilon_0 + \delta \ln t + \phi t \quad \text{or}$$
$$\varepsilon = \varepsilon_0 + \vartheta t^{1/3} + \phi t, \tag{1}$$

where ε_0 is the immediate strain and δ, ϑ, and ϕ are creep
coefficients [3]. After a short transient phase ("primary
creep"), approximated as logarithmic ($\sim\delta \ln t$) or using
Andrade's law ($\sim\vartheta t^{1/3}$), this describes a steady-state
"secondary" creep, dominated by the last term, where
the rate ϕ is determined by the balance of work hardening
and thermal softening. Under such circumstances the
steady state creep is fairly well represented by the
Norton equation:

$$\dot{\varepsilon} = \frac{\partial \varepsilon}{\partial t} = C(T)\sigma^\alpha, \tag{2}$$

where σ is the stress in the system, $C(T)$ is a factor
characteristic for the material and the experimental con-
ditions (temperature, grain size of a polycrystalline sample,
Young modulus, etc.), and α is the Norton exponent with
$1 \leq \alpha \leq 10$ (from experiment, depending on the dominat-
ing microscopic process). Simplified theoretical models
reduced to thermal activation of independent dislocation
glide movements in the lattice (Harper-Dorn creep) predict
an exponent $\alpha = 1$ in Eq. (2) [3–6]. This phenomenological
description was derived mostly for tension strain, but can
be applied for shear (along the x axis in our notation) as
well, with the substitution $\varepsilon \rightarrow \gamma$, where $\gamma = \partial x/\partial y$ and

$\dot{\gamma} = \partial v_x / \partial y$. In the case of large grained pure materials (mostly metals) at intermediate stresses and temperatures, the deformation is realized by the creation and glide movement of edge dislocations with Burgers vectors $\vec{b}$, resulting in shear rates $\dot{\gamma} = \rho \vec{b} \vec{v}$ (Orowan equation), where ρ is the density of mobile dislocations with average velocity $\vec{v}$. In this model the dislocation density ρ is expected to depend on the shear stress as

$$\rho \propto \sigma^\beta. \tag{3}$$

Simple theoretical arguments and tensile experiments on single and polycrystalline copper predict an exponent $\beta \approx 2$ [7].

The effects of shearing forces and liquid state viscosity were investigated in early years of dusty plasma research [8–11]. More recently, effects of shearing forces on the microstructure were experimentally investigated in greater detail including liquid flows and plastic deformations of a crystalline solid [12–17]. Here we present dusty plasma experiments providing the link between the standard, macroscopic measures used in material sciences and metallurgy to describe plastic deformations, and the detailed microscopic information provided by dusty plasma experiments.

We have carried out two independent experiments on single layer crystalline dusty plasma systems aiming to investigate the microscopic details of the shearing creep deformation. The first experiment was performed in the Hypervelocity Impacts and Dusty Plasmas Lab (HIDPL) of the Center for Astrophysics, Space Physics, and Engineering Research (CASPER) at Baylor University, Waco, Texas, while the second series was carried out at the Institute for Solid State Physics and Optics, part of the Wigner Research Centre for Physics, Budapest, Hungary (referenced as "TEX" and "BUD" in the following). Details of the dusty plasma apparatuses and data processing techniques can be found in earlier publications [16,18]. In both cases the dust layer was illuminated by an extended, spatially linearly modulated laser sheath introducing an external force $F_x(y) = F_0(y - y_0)$ on every particle, as illustrated in Fig. 1.

Several video sequences with different powers of the manipulating laser P_L were recorded, including the $P_L = 0$ case, which was used to extract the wave spectra of thermally excited density fluctuations, which fitted with lattice phonon dispersion curves of 2D Yukawa systems [19,20] resulted in system parameters used during the evaluation of the $P_L > 0$ data. These parameters are collected in Table I.

The elementary steps of the data evaluation process are illustrated in Fig. 2 and include (a) the identification of the particles and determination of the regions of interest, (b) measurement of the pair distribution function $g(r)$, (c) performing Delaunay triangulation to determine true
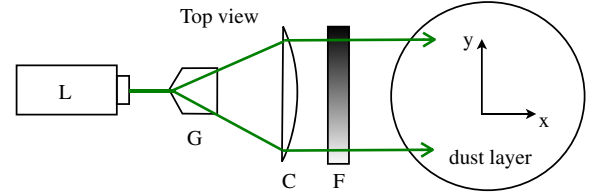

FIG. 1 (color online). Scheme of the optical setup used to generate the wide shearing laser beams. Main parts: L, laser source (TEX, max 5.5 W @ 532 nm; BUD, max 1 W @ 440 nm); G, laser line generator lens; C, cylindric lens; F, linearly variable density filter.

nearest neighbor bonds and identify defects, defined as particles with neighbor numbers $\neq 6$. The measurement of the particle velocities includes the determination of flow, peculiar and particular thermal velocities. Examples of the induced flow velocity profiles $v_x(y)$ for laser intensities in the range of $0.4 \cdots 5$ W are presented in Fig. 2(d), showing a pronounced difference between the two experiments. Linear velocity profiles were found in the TEX case, while in the BUD experiments the velocity profiles decayed exponentially. To benefit from both situations we have defined the regions of interest [marked with red lines in Fig. 2(a)]. In the case of TEX, to avoid complication with the boundaries (including circulations) of the dust clouds during the subsequent evaluation steps we consider only particles within a circle with a diameter of about 75% of that of the cloud. The shear rate $\dot{\gamma} = \partial v_x / \partial y$ is constant

TABLE I. System parameters derived from the structural and dynamical properties of the unperturbed systems. Uncertainties are estimated to vary from 1% (e.g., m, d, resolution) up to 10% (e.g., q, κ).

| Parameter	TEX	BUD
p, Ar gas pressure [Pa]	9.6	1.25
$P_{\rm rf}$, rf power at 13.56 MHz [W]	3.5	15
d, MF particle diameter [μm]	6.37	9.16
m, particle mass [10^{-13} kg]	2.04	6.08
N, particle number in field of view	1404	2810
Frames per second (fps)	60	29.7
Recorded frames per experiment	5500	17 000
Resolution [μm/pixel]	35.2	30
q, charge (e, elementary charge)	7250	13 600
n, density [10^6 m^{-2}]	2.76	2.99
a, Wigner-Seitz radius [10^{-4} m]	3.4	3.26
$\omega_p = q\sqrt{n/2\varepsilon_0 ma}$ [rad/s]	55.1	63.5
λ_D, Debye screening length [10^{-4} m]	4.9	4.8
$\kappa = a/\lambda_D$, Yukawa parameter	0.7	0.68
$T/T_{\rm melt}$ from $g(r)$, see Ref. [21]	0.42	0.37
$v_{\rm th}$, average thermal speed [10^{-4} m/s]	12.7	4.46
$\dot{\gamma}_0 = v_{\rm th}/a$ [s^{-1}]	3.74	1.37
$\sigma_0 = mn\omega_0 av_{\rm th}$ [10^{-11} kg/s^2]	1.34	1.68

Note: MF means Melamine-formaldehyde.
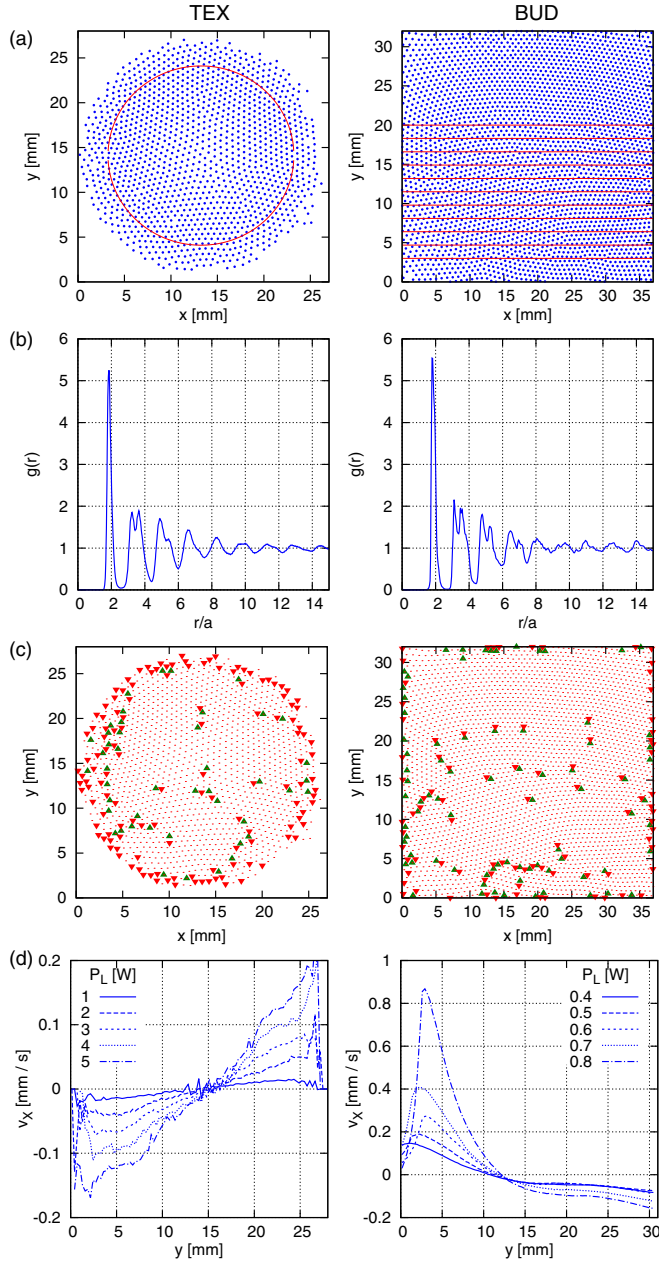
FIG. 2 (color online). Illustration of the data evaluation process for both experiments (left column, TEX; right column, BUD). For the unperturbed cases, (a) example of particle snapshots with the regions of interest, (b) pair correlation function, (c) defect maps (upper triangle, particle with seven neighbors; lower triangle, particle with five neighbors). (d) $v_x(y)$ transverse particle velocity profiles for different shearing laser powers.

over the whole y range. In the case of BUD. as the dust cloud is much larger than the field of view of the camera, boundary effects are of minor concern. On the other hand, the velocity profiles show strong nonlinear shape. We define ten slabs within the decaying tail [see Fig. 2(a) right column] of $v_x(y)$, where the shear rate within each slab can be approximated as constant, but it changes from slab to slab, providing the possibility of evaluating ten

different $\dot{\gamma}$ values at once. The qualitative difference of the velocity profiles is assumed to be related to the significantly different Ar gas pressures, which, through friction, is responsible for the energy dissipation.

The two quantities of interest, besides the directly measured shear rate, are the defect fraction (proportional to the dislocation density) and the shear stress in the system. The former results from the Delaunay triangulation. The latter is computed applying the formula

$$\sigma_{xy} = \frac{1}{A}\left[\sum_i m v_{i,x} v_{i,y} + \frac{1}{2}\sum_i \sum_{j \neq i} r_{ij,y} F_{ij,x}\right], \quad (4)$$

where A is the area of the region of interest, $v_{i,x}$ is the x component of the peculiar velocity of particle i, $r_{ij,y}$ is the y component of the distance vector between particles i and j, and $F_{ij,x}$ is the x component of the force acting on particle i due to pair interaction with particle j. Summation over i is for particles within A, while summation of j runs over all particles interacting with particle i. To approximate the interparticle forces, we use the widely accepted Yukawa (screened Coulomb) model, with a pair potential: $\Phi(r) = q \exp[-r/\lambda_D]/(4\pi\varepsilon_0 r)$, where q is the charge of the dust particle, λ_D is the Debye screening length, and ε_0 is vacuum permittivity. The values of these quantities are listed in Table I.

The results of the data evaluation are presented in Fig. 3. The experimental data points are approximated by functions having the forms

$$D(\dot{\gamma}) = D_0 + d\dot{\gamma}^b \quad \text{and} \quad \sigma(\dot{\gamma}) = c\dot{\gamma}^f. \quad (5)$$
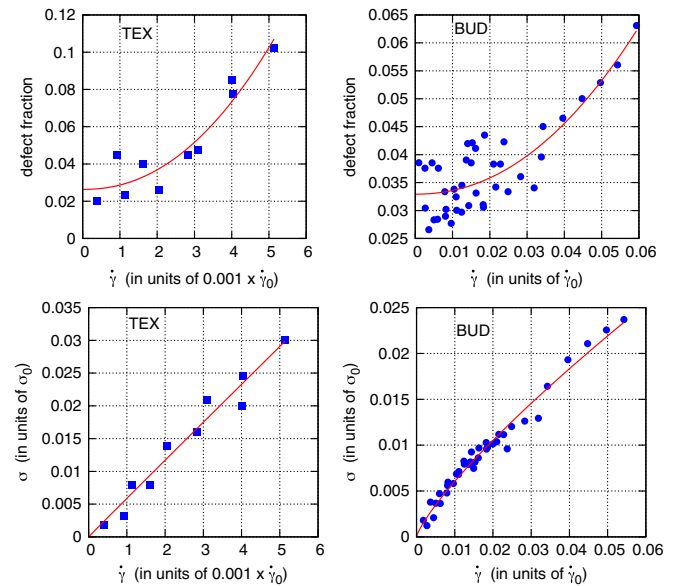

FIG. 3 (color online). Defect fraction (upper row) and shear stress (lower row) versus shear rate from both the TEX (left column) and BUD (right column) experiments. Lines are functional fits, see text.
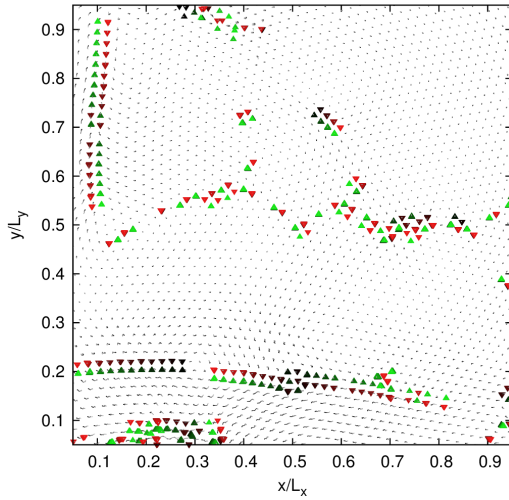
FIG. 4 (color online). Defect maps of subsequent system snapshots from the BUD experiment. Colors lighten with elapsing time. upper triangle, particles with seven neighbors; lower triangle, particles with five neighbors.
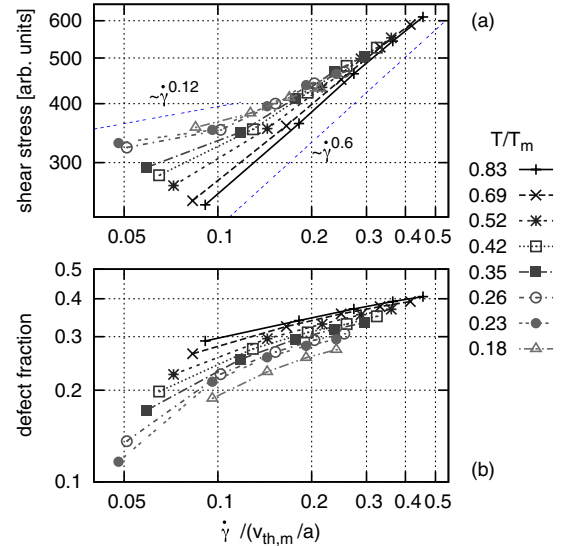

FIG. 5 (color online). Computed shear stress (a) and defect fraction (b) versus shear rate for a set of homologous temperatures. The bounding dotted lines in (a) show simple power law functions with exponents as labeled.

In a polycrystalline system at finite temperature, even without external shear, the equilibrium defect (dislocation) density D_0 is nonzero, in contrast to the shear stress. D_0 corresponds to the immobile fraction of the dislocations, which are excluded from Eq. (3). Least-squares fitting resulted in $b_{\text{TEX}} = 2.15 \pm 0.5$, $b_{\text{BUD}} = 2.1 \pm 0.3$, $f_{\text{TEX}} = 0.95 \pm 0.1$, $f_{\text{BUD}} = 0.8 \pm 0.03$ for the exponents. Combining these results, we find that the defect density—shear stress relation, as given in Eq. (3), is, at least in the studied shear rate regime, a good approximation and has an exponent $\beta = b/f \approx 2.4 \pm 0.4$. Furthermore, the Norton exponent in Eq. (2) is $\alpha = 1/f \approx 1.15 \pm 0.1$. These results are consistent with both (BUD and TEX) experiments. Taking into account the fact that the crystalline domains are large, compared to the system size, these values of the exponents suggest the Harper-Dorn creep [3–5] to be the dominant process.

To support this statement, Fig. 4 shows an overlay of subsequent defect maps (BUD, $P_L = 0.6$ W). This illustrates the formation and rapid glide of dislocation pairs through the lattice, a typical scenario occurring frequently in the system. In frustrated dusty plasma crystals such individual processes have already been observed [22,23] and studied numerically in detail [24].

In addition to dusty plasma experiments, nonequilibrium molecular dynamics simulations [25] for a 2D particle ensemble with $N = 46\,000$ particles were conducted, again assuming a Yukawa interparticle interaction potential. Particles were placed randomly in a rectangular simulation box to match the ground state hexagonal lattice. After a thermalization period, a homogeneous shear algorithm was applied to generate planar Couette flow [26]. In the algorithm the shear flow is induced with the Lees-Edwards (sliding brick) periodic boundary conditions, which is used

in conjunction with the Gaussian thermostatted SLLOD equations of motion:

$$\frac{d\mathbf{r}_i}{dt} = \frac{\tilde{\mathbf{p}}_i}{m} + \dot{\gamma} y_i \hat{\mathbf{x}}, \qquad \frac{d\tilde{\mathbf{p}}_i}{dt} = \mathbf{F}_i - \dot{\gamma} \tilde{\mathbf{p}}_{yi} \hat{x} - \tau \tilde{\mathbf{p}}_i, \qquad (6)$$

where $\tilde{\mathbf{p}} = (\tilde{p}_x, \tilde{p}_y)$ is the peculiar momentum of particles, $\hat{\mathbf{x}}$ is the unit vector in the x direction, and τ is the Gaussian thermostatting multiplier, calculated in a way to ensure constant peculiar kinetic energy. The integration of this set of equations is solved by the operator-splitting technique [27]. During the simulations we track the positions and velocities of particles and perform the analysis already introduced for the experiments.

The simulations require as dimensionless input parameters the homologous temperature T/T_m, and $\tilde{\dot{\gamma}} = \dot{\gamma}(a/v_{\text{th},m})$, where $v_{\text{th},m} = \sqrt{2k_B T_m/m}$ is the thermal velocity at melting temperature. Calculations are performed for Yukawa screening parameter $\kappa = a/\lambda_D = 2$, $T/T_m = 0.18 \cdots 0.83$, and $\tilde{\dot{\gamma}} = 0.05$–$0.5$.

Figure 5 shows the computed shear stress and defect fraction values versus the strain rate for a set of homologous temperatures. The shear stress curves in Fig. 5(a) asymptotically join to a universal power-law function with a Norton exponent of $\alpha \approx 1/0.6 \approx 1.7$ at high shear rates. The effect of temperature is most dominant at low shear rates, where the system hardens with decreasing temperature, while reaching Norton exponents up to $\alpha \approx 1/0.12 \approx 8$ at the lowest investigated temperature. The defect fraction in Fig. 5(b) shows a similar, but somewhat weaker asymptotic trend. The tendency of developing fewer defects at lower temperatures in a steady-state configuration still dominates over the effect of the external frustration.

In summary, we have experimentally determined the plastic properties of 2D dusty plasma single layers in the polycrystalline phase. The macroscopic measures, like the defect density—shear stress relation and Norton exponent during slow deformations (creep) are fully coherent with empirical models used to describe ordinary materials. This fact supports the concept of using dusty plasmas as magnified model systems of ordinary matter and provides the possibility of studying a wide variety of many-body phenomena on the particle (quasiatomic) level with spatial and temporal resolutions easily accessible on the human scale.

[1] P. Tan, N. Xu, and L. Xu, Nat. Phys. **10**, 73 (2014).
[2] P. Hartmann, Z. Donkó, T. Ott, H. Kählert, and M. Bonitz, Phys. Rev. Lett. **111**, 155002 (2013).
[3] A. H. Cottrell, *The Mechanical Properties of Matter* (John Wiley and Sons, New York, 1964).
[4] J. G. Harper, L. A. Shepard, and J. E. Dorn, Acta Metall. **6**, 509 (1958).
[5] O. Ruano, J. Wadsworth, and O. Sherby, Acta Metall. **36**, 1117 (1988).
[6] M. Kassner, P. Kumar, and W. Blum, Int. J. Plast. **23**, 980 (2007).
[7] T. H. Courtney, *Mechanical Behavior of Materials* (McGraw-Hill, New York, 1990).
[8] W.-T. Juan, M.-H. Chen, and Lin I, Phys. Rev. E **64**, 016402 (2001).
[9] V. Nosenko and J. Goree, Phys. Rev. Lett. **93**, 155004 (2004).
[10] A. Gavrikov, I. Shakhova, A. Ivanov, O. Petrov, N. Vorona, and V. Fortov, Phys. Lett. A **336**, 378 (2005).
[11] Z. Donkó, J. Goree, P. Hartmann, and K. Kutasi, Phys. Rev. Lett. **96**, 145003 (2006).
[12] C.-L. Chan and L. I, Phys. Rev. Lett. **98**, 105002 (2007).
[13] C.-W. Io and L. I, Phys. Rev. E **80**, 036401 (2009).
[14] C. Durniak and D. Samsonov, Phys. Rev. Lett. **106**, 175001 (2011).
[15] V. Nosenko, A. V. Ivlev, and G. E. Morfill, Phys. Rev. Lett. **108**, 135005 (2012).
[16] P. Hartmann, M. C. Sándor, A. Kovács, and Z. Donkó, Phys. Rev. E **84**, 016404 (2011).
[17] V. Nosenko, A. V. Ivlev, and G. E. Morfill, Phys. Rev. E **87**, 043115 (2013).
[18] C. M. Boessé, M. K. Henry, T. W. Hyde, and L. S. Matthews, Adv. Space Res. **34**, 2374 (2004).
[19] F. M. Peeters and X. Wu, Phys. Rev. A **35**, 3109 (1987).
[20] P. Hartmann, Z. Donkó, G. Kalman, S. Kyrkos, M. Rosenberg, and P. Bakshi, IEEE Trans. Plasma Sci. **35**, 337 (2007).
[21] T. Ott, M. Stanley, and M. Bonitz, Phys. Plasmas **18**, 063701 (2011).
[22] V. Nosenko, S. Zhdanov and G. Morfill, Phys. Rev. Lett. **99**, 025002 (2007).
[23] C. Durniak, D. Samsonov, J. F. Ralph, S. Zhdanov, and G. Morfill, Phys. Rev. E **88**, 053101 (2013).
[24] S. K. Zhdanov, M. H. Thoma, C. A. Knapek, and G. E. Morfill, New J. Phys. **14**, 023030 (2012).
[25] D. C. Rapaport, *The Art of Molecular Dynamics Simulation* (Cambridge University Press, Cambridge, England, 2004).
[26] D. J. Evans and G. P. Morriss, *Statistical Mechanics of Nonequilibrium Liquids* (Academic Press, New York, 1990).
[27] G. Pan, J. F. Ely, C. McCabe, and D. J. Isbister, J. Chem. Phys. **122**, 094114 (2005).